Ab initio calculation of the phonon dispersion of antimony-covered (110) surfaces of III-V compounds

J. Fritsch, M. Arnold, and U. Schröder
Institut für Theoretische Physik, Universität Regensburg, D-93040 Regensburg, Germany
(Received 21 January 2000)

We present the results from *ab initio* linear-response calculations performed to investigate the surface phonon dispersion of the antimony-covered (110) surfaces of GaAs, GaP, InAs, and InP. Our computations are carried out for a complete monolayer coverage of antimony adsorbed in the epitaxial continued layer structure. The surfaces are described within the slab-supercell approach. Our density-functional formalism is based on the plane-wave pseudopotential method and the local-density approximation. We identify characteristic vibrations of the adsorption overlayer, interface modes, and phonons related to those of the pristine surfaces with changed dispersion due to the adsorption. A comparison of the modes computed for the different systems allows us to analyze systematic trends and to study more thoroughly the physical origin of vibrational states occurring on adsorbate-covered and clean III-V(110) surfaces. Our computed phonon frequencies are in good agreement with experimental data.

I. INTRODUCTION

The physical and chemical properties of interfaces between metals and semiconductors attract much attention from the viewpoint of fundamental research and because of their technological importance. On (110) surfaces of several III-V compound semiconductors, antimony is known to form well-ordered epitaxial overlayers. Therefore, a large number of experimental data exists for antimony-covered GaAs, GaP, and InP(110). These surfaces are ideal systems for investigating the structure and electronic properties of single adsorption layers. By means of low-energy electron diffraction (LEED), Auger-electron spectroscopy, and photoemisson spectroscopy, it was shown that the adsorption of Sb on the (110) surfaces of GaAs, GaP, InAs, and InP can be brought to saturation with two atoms per surface unit cell. The adsorption layer shows well-ordered (1×1) symmetry.[1–4]

Antimony is an exceptionally well-behaved adsorbate. Annealing at moderate temperature increases the quality of deposited Sb films and leads to essentially ideal (1×1) termination.[5–9] For the adsorption of Sb detailed data are mainly available for GaAs, GaP, InAs, and InP(110) from LEED, surface extended x-ray adsorption fine structure (SEXAFS), photoemission diffraction (PED), and grazing-incidence x-ray diffraction (GIXD).[4,7,10–16] In total-energy calculations several models were proposed for the structure of the one-monolayer adsorption geometry.[17–22] The theoretical studies show that the epitaxial continued layer (ECL) structure is the geometry with the lowest energy. This is consistent with the good agreement of the values computed for the relaxation parameters with those determined in experiments.[4,7,10–16]

In the course of the last decade, the vibrational features of the interface and of the adsorption layer could be measured with increasing precision by means of Raman spectroscopy.[23–27] The data provide important new information for a conclusive clarification of the surface atomic structure of the (1×1) geometry. So far, only a few computations were done to determine vibrational features characterizing the Sb:III-V(110) surfaces.[21,22,28–31] The studies that were carried out on the basis of restricted dynamical models gave phonon energies of zone-center modes. The results from recent Raman scattering experiments performed with substantially enhanced resolution[32] and the measurement of complete dispersion curves by means of inelastic helium-atom scattering[33] (HAS) give stimulating new impulses for comprehensive theoretical studies. There is a need for the computation of complete phonon dispersion curves, using a method that includes all degrees of freedom to describe the vibrations of the atoms.

Here, we report the results from *ab initio* linear-response calculations performed to determine the vibrational modes of Sb adsorbed in the ECL structure on the (110) surfaces of GaAs, GaP, InAs, and InP. Only for these Sb:III-V(110) systems are measured phonon frequencies available. We use density-functional perturbation theory[34,35] (DFPT) applied to periodically repeated crystal films. In contrast with previous investigations, complete phonon dispersion curves are determined by calculating the slab modes without any restriction of the dynamics.

The vibrational states of Sb on III-V(110) surfaces are not only of interest in order to understand the structure of the adsorption systems more thoroughly. They are also helpful to study in more detail the phonon modes of the clean surfaces. Some vibrational features of the pristine surface were discussed in a controversial way. One important example is a mode that may be considered to be the dynamical analog of the surface relaxation. The tight-binding total-energy calculations of Wang and Duke predicted a surface vibrational feature characterized by nearly bond-length-conserving rotations that change the tilt angle of the surface anion-cation chains.[36] For GaAs(110) this mode was assigned to the flat branch previously resolved at about 10 meV by means of HAS experiments.[37,38] In a series of computations,[39–41] an explanation similar to that given by Wang and Duke was provided for the experimentally observed branch. Theoretical

TABLE I. Lattice constant a_0 (in Å) of zinc-blende-phase GaP, GaAs, InP, and InAs. Our results are compared with those of the DFT calculation of Ref. 55 and the experimental data compiled in Ref. 35.

	GaP	GaAs	InP	InAs
This work	5.411	5.613	5.802	5.980
DFT	5.359	5.559	5.662	5.861
Expt.	5.451	5.654	5.869	6.036

studies that accounted for the coupling of surface modes with bulk phonons gave vibrational states of this kind. However, the computed phonon modes were found to be largely resonant with bulk vibrations. Hence, no clear identification of the rotational mode was possible.[42–46]

Another interesting topic is the behavior of the gap phonon modes found for compounds such as GaP and InP, which show a large separation between their acoustic and optical bulk mode frequencies. Previous computations predicted substantial shifts of the gap mode energies resulting from changes of the relaxation angle. The frequency shifts determined for the ideal unrelaxed surfaces were consistent with those found for hydrogen coverages.[43,44,47] Unfortunately, hydrogen exposure leads to surface-etching chemical reactions. Therefore it is not possible to verify experimentally the predictions from theory by means of hydrogen adsorption. Overlayers of Sb, however, stabilize the III-V(110) surfaces. The possibility to prepare monolayer coverages with excellent structural quality emphasizes that Sb is an ideal adsorbate to be used in measurements that probe adsorption-induced frequency shifts of the gap modes.

II. THEORETICAL METHOD

Our computations are based on density-functional theory[48] (DFT) applied in the local-density approximation.[49] For the exchange-correlation potential we use the form proposed by Ceperley and Alder[50] in the parametrization suggested by Perdew and Zunger.[51] The electron-ion interaction is described by norm-conserving nonlocal pseudopotentials.[52–54] The electronic wave functions are expanded in plane waves up to a maximal cutoff energy of 10 Ry for Sb adsorbed on GaAs, InAs, and InP(110) and 11 Ry for Sb on GaP(110).

To apply the plane-wave formalism to the (110) surfaces of III-V semiconductors, we introduce periodically repeated thin crystal films, fixing the lattice constant at the theoretical value determined for the bulk of GaAs, GaP, InAs, and InP as listed in Table I, which shows that our computed lattice constants are in good agreement with experimental data. The slabs contain a total of nine atomic layers, which comprise seven substrate layers and one monolayer of Sb adsorbed on either of the two surfaces of each crystal film. Two neighboring slabs are separated by a distance that is equal to three removed atomic (110) layers. The thickness of the slabs and their separation guarantee that the interaction of neighboring crystal films is negligible and that the surfaces of each slab are sufficiently decoupled. For the **k**-point sampling we use six special points in the irreducible part of the surface Brillouin zone. The equilibrium positions of Sb adsorbed in the ECL structure are determined by minimizing the total energy with the help of the Hellmann-Feynman forces, starting the atomic relaxation from the ideal positions derived from the symmetry of the bulk. Each atom is allowed to move with the exception of the central-layer atoms. The relaxation is stopped when all forces are smaller than 0.1 mRy/a.u. This defines the computed equilibrium positions with a numerical uncertainty of less than 0.01 Å. For the determination of realistic surface geometries, it is necessary to calculate bond lengths with sufficient accuracy. This is achieved in our computations as reflected by the agreement of our lattice constants with measured data and the results summarized in the next section.

The phonon dispersion is determined by means of density-functional perturbation theory (DFPT) using the formalism of Baroni and co-workers.[34,35] We calculate dynamical matrices for entirely relaxed nine-layer slabs by determining the static linear response of the electrons for periodic displacements of the atoms from their equilibrium positions. Screening through the electrons is included by computing the first-order variation of the charge density in an iterative scheme, until self-consistency is achieved for the variation of the linear response of the electrons and the screened perturbing potential. In order to determine the complete phonon dispersion along and perpendicular to the Sb chains of the ECL structure, dynamical matrices are calculated at four points in the $\overline{\Gamma X}$ and three points in the $\overline{\Gamma X'}$ direction of the surface Brillouin zone. The dynamical matrices at arbitrary wave vectors can be evaluated with the help of Fourier deconvolution. In order to identify resonances and deeply penetrating surface states, we construct the dynamical matrices of larger slabs comprising 25 atomic layers. The force constants in the surface region of the large crystal films are assumed to be the same as the respective force constants in the nine-layer slabs. For the inner region of the large crystal films, we use bulk force constants.

III. SURFACE RELAXATION OF THE EPITAXIAL CONTINUED LAYER STRUCTURE

Several structural models were proposed for the adsorption of Sb on the (110) surfaces of GaAs, GaP, InAs, and InP. A detailed compilation of experimental and theoretical work done to determine the surface geometry of a complete monolayer with (1×1) periodicity is given in Ref. 22. Investigations of the adsorption of group-V elements on (110) surfaces of other III-V compounds were essentially restricted to Bi:GaSb(110). In a series of total-energy calculations performed for Sb adsorbed on GaAs, GaP, InAs, and InP,[17–22] the ECL structure was found to be the most favorable model. Other geometries such as the p^3 structure, the epitaxial on-top structure, the epitaxial overlapping chain structure, and the dimer model (see Fig. 11 of Ref. 22) gave higher surface energies. In the ECL geometry, two Sb atoms are adsorbed per (1×1) unit cell of the pristine surface, occupying all atomic positions of the ''next lattice layer'' derived from the symmetry of the underlying material. By this, the Sb atoms are arranged in chains along the $[1\bar{1}0]$ direction. Each Sb atom is bonded to one atom of the substrate and the two neighboring Sb atoms in its chain. The structural parameters and the zone-center frequencies of highly localized surface

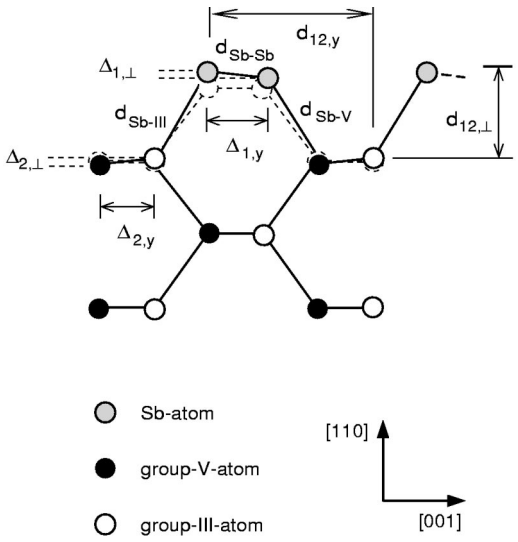

FIG. 1. Side view of the relaxed ECL structure of Sb covering the (110) surfaces of III-V compound semiconductors. The structural parameters determined for the adsorption on GaAs, GaP, InAs, and InP are summarized in Tables II and III. The dotted circles indicate the ideal positions derived from the symmetry of the bulk.

vibrations computed for the ECL structure[21,22] compare very well with experimental data.[10,12,13,24,26,27] Therefore, it is now well established that the one-monolayer adsorption of Sb on the (110) surfaces of GaAs, GaP, InAs, and InP results in the ECL structure.

Figure 1 illustrates the atomic positions in the ELC geometry and some of its characteristic structural parameters. Tables II and III summarize our values computed for the relaxation parameters and compare the data with those of experimental investigations[10,12,13] and the results of the DFT calculations of Schmidt and co-workers.[21,22] The measured relaxation parameters are well reproduced by our calculations and those of Refs. 21 and 22. Some of the experimental data compare better with our results, while other are in better agreement with those of Schmidt and co-workers. As can be seen from the figure, the relaxation of the clean (110) surfaces is removed and replaced by a slight counter-rotation of the anion-cation chains in the first substrate layer. The Sb-Sb chains formed by the overlayer atoms are tilted in a similar way as the first-layer zigzag chains of the respective clean surfaces. However, the relaxation angle of the adsorption layer is distinctly smaller.

TABLE II. Structural parameters (in Å) of one monolayer of Sb adsorbed in the ECL structure on the (110) surfaces of GaAs, GaP, InAs, and InP. The parameters are defined in Fig. 1. Our results are compared with those of the DFT calculation of Ref. 21 and experimental data taken from Refs. 10, 12, and 13.

Surface	Reference	$\Delta_{1,\perp}$	$\Delta_{1,y}$	$d_{12,\perp}$	$d_{12,y}$	$\Delta_{2,\perp}$	$\Delta_{2,y}$
Sb:GaAs	This work	0.07	2.00	2.39	4.50	0.09	1.43
	DFT [a]	0.05	2.00	2.37	4.52	0.09	1.41
	LEED [b]	0.08	1.99	2.34		0.11	1.40
Sb:GaP	This work	0.12	1.99	2.39	4.32	0.07	1.38
	DFT [a]	0.10	2.03	2.38	4.34	0.07	1.35
	PED [c]	0.07	1.91	2.32	4.56		
Sb:InAs	This work	0.16	1.93	2.41	4.61	0.11	1.57
	DFT [a]	0.12	1.94	2.31	4.63	0.08	1.51
	PED [d]	0.10	1.93	2.39			
Sb:InP	This work	0.20	1.96	2.43	4.47	0.10	1.52
	DFT [a]	0.16	1.98	2.44	4.44	0.07	1.46
	PED [c]	0.13	1.87	2.41	4.59		

[a]Reference 21.
[b]Reference 10.
[c]Reference 12.
[d]Reference 13.

TABLE III. Bond lengths (in Å) of the adsorption system and the substrate determined for Sb covering GaAs, GaP, InAs, and InP(110) in the one-monolayer ECL structure. Our results are compared with those of Ref. 22 and the experimental data of Refs. 10, 11, and 15. The sum Σr_{cov} of the covalent radii is summarized for each bond.

Surface	Reference	$d_{\mathrm{Sb\text{-}Sb}}$	$d_{\mathrm{Sb\text{-}V}}$	$d_{\mathrm{Sb\text{-}III}}$	$d_{\mathrm{III\text{-}V}}$
Sb:GaAs	This work	2.82	2.64	2.62	2.43
	DFT (Ref. 22)	2.81	2.66	2.59	2.41
	LEED (Ref. 10)	2.77	2.66	2.64	
	Σr_{cov}	2.80	2.60	2.66	2.46
Sb:GaP	This work	2.77	2.52	2.62	2.34
	DFT (Ref. 22)	2.78	2.55	2.59	2.32
	SEXAFS (Ref. 15)	2.88	2.60	2.79	
	Σr_{cov}	2.80	2.46	2.66	2.26
Sb:InAs	This work	2.87	2.62	2.77	2.59
	DFT (Ref. 22)	2.84	2.66	2.72	2.54
	Σr_{cov}	2.80	2.60	2.84	2.70
Sb:InP	This work	2.84	2.52	2.77	2.51
	DFT (Ref. 22)	2.82	2.55	2.72	2.45
	LEED (Ref. 11)	2.82	2.52	2.80	
	Σr_{cov}	2.80	2.46	2.84	2.50

The magnitude of the tilt angle essentially reflects the difference between the Sb-anion and Sb-cation bond lengths. This can be seen from the parameters $\Delta_{1,\perp}$, $d_{\mathrm{Sb\text{-}V}}$, and $d_{\mathrm{Sb\text{-}III}}$ compiled in the tables. Schmidt and Srivastava pointed out that the vertical shear $\Delta_{1,\perp}$, which characterizes the adsorption structure, increases steadily with the inequivalence of the substrate atoms.[21] The authors of Ref. 21 found that the overlayer buckling varies nearly linearly with the relative difference of the tetrahedral radii and also with the charge asymmetry between the group-III and group-V atoms of the substrate. The experimental data show a similar behavior with the exception of Sb:GaAs(110).

Another parameter that exhibits a systematic trend is the bond length $d_{\mathrm{Sb\text{-}Sb}}$ between neighboring adlayer atoms along the chains. In good agreement of our results with those of Schmidt and Srivastava, which are slightly closer to the experimental data, we find that the value computed for $d_{\mathrm{Sb\text{-}Sb}}$ increases with the lattice constant of the substrate, as can be

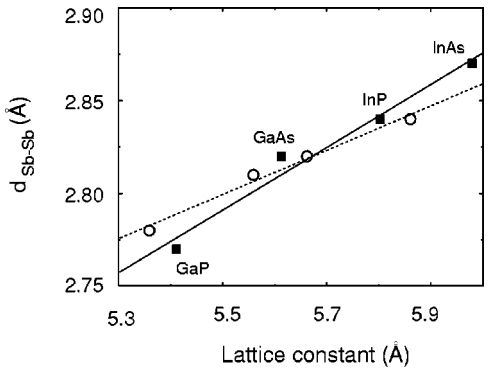

FIG. 2. Sb-Sb bond length computed for the Sb adlayer on the (110) surfaces of GaP, GaAs, InP, and InAs as a function of the calculated lattice constant. Our results are indicated by filled squares. Empty circles represent the results of Ref. 22. The lines result from a linear fit to our data (solid line) and those represented by the circles (dotted line).

seen from Tables I and III and from Fig. 2. The bond length $d_{\text{Sb-Sb}}=2.88$ Å determined by SEXAFS for Sb:GaP(110) (Ref. 15) is significantly larger than the data measured by LEED for Sb on GaAs and InP(110).[4,10] While the bond length between the adatoms is dependent on the substrate lattice constant, the bond lengths $d_{\text{Sb-III}}$ and $d_{\text{Sb-V}}$ between Sb and the substrate atoms are essentially independent on the particular compound. Our computed values for $d_{\text{Sb-Ga}}$, $d_{\text{Sb-In}}$, and $d_{\text{Sb-P}}$ are 2.62, 2.77, and 2.52 Å. For the adsorption of Sb on GaAs and InAs(110), we obtain 2.64 and 2.62 Å for $d_{\text{Sb-As}}$. The sharp difference between the behavior of the Sb-Sb bond lengths one the one hand and that of the adlayer-substrate bond lengths on the other indicates that the bonds between neighboring Sb atoms are weaker than the bonds between the adlayer and the substrate. A comparison with the bulk-bond lengths $d_{\text{III-V}}$ also compiled in Table III shows that $d_{\text{Sb-Sb}}$ is always larger than $d_{\text{III-V}}$. This indicates that the Sb atoms are displaced from the ideal ECL positions parallel to the surface and perpendicular to the Sb-Sb chains.

IV. SURFACE PHONON DISPERSION

The ECL adsorption geometry closely resembles the bulk-derived structure. Hence, the cation-bonded Sb atoms are adsorbed in an anionlike environment, while the anion-bonded Sb atoms occupy the cation sites in the layer above the surface. The vibrational features of a Sb:III-V(110) surface therefore comprise oscillations of adlayer atoms, interface phonons, and phonon modes that correspond to vibrations of the pristine surface.

The epitaxial continuation of the substrate in the ECL structure allows one to investigate the influence of the adsorption layer on the dispersion of acoustic phonon modes. The Sb-overlayer atoms have a larger mass than the atoms of the underlying material. Therefore, a significant reduction of the frequencies of some modes like the Rayleigh wave has to be expected. As a result of the adsorption, the relaxation of the substrate is removed and replaced by a slight counter-relaxation. For the adsorption of hydrogen, which leads to a similar derelaxation of the clean (110) surfaces, it was predicted by previous DFPT studies that the frequencies of the modes lying in the gap between the acoustic and optical bulk vibrations change drastically.[44,47] However, hydrogen exposure is disadvantageous because of its surface etching behavior. The feasibility of Sb-overlayer preparation finally allows one to investigate experimentally relaxation-angle dependent frequency shifts of modes as already predicted for the clean InP(110) surface.[43]

Figures 3, 4, 6, and 7 illustrate the phonon dispersion computed for the ECL structure of Sb on the (110) surfaces of GaAs, GaP, InAs, and InP. Our results are compared with data from Raman spectroscopy and frozen-phonon calculations,[21,24,25,27] which were restricted to the determination of zone-center modes. For wave vectors along the $\overline{\Gamma X'}$ direction, the vibrational states are strictly separated into A' modes purely polarized in the sagittal plane and A'' modes that have atomic displacements only parallel to the adlayer zigzag chains. Also included in the figures are characteristic phonon modes of the uncovered surfaces (dotted lines).

The triangles in the figures represent the results form the frozen-phonon calculations of Schmidt and Srivastava. They studied the vibrational modes on the base of a restricted dynamical model using the force constants computed for atomic displacements in the outer three layers. The authors considered phonon modes localized in the adlayer and in the first substrate layer. Ideally, this yields six A' and three A'' modes. The frequencies of well-localized modes can be determined with sufficient accuracy by this approach. The energies of vibrational states with deep penetration, however, can only be estimated. Moreover, it is not possible to distinguish between really surface-localized vibrational features and bulklike modes in restricted dynamical models. There is no strict relation between the number of atoms in the surface region and the number of surface states that can be detected. Most of the phonon modes determined in the frozen-phonon calculation correspond to vibrational features determined by our computations. However, some modes have distinctly different frequencies or are not surface localized according to our calculations. Before we focus on a compilation of similar features that are present in all phonon spectra, our results obtained for the individual surfaces are summarized and compared with experimental findings.

A. Phonon dispersion of Sb:GaAs(110)

Figure 3 illustrates the phonon dispersion determined for Sb:GaAs(110). At the $\overline{\Gamma}$ point, we obtain five strongly localized phonon modes with energies of 9.5, 22.4, and 26.6 meV for three vibrations with A' character and 19.7 and 29.3 meV for two A'' modes. Hence, the vibrational states detected by Raman scattering[24,25] at 9.2, 20.6, and 22.3 meV can be identified as surface-localized modes in our computations. However, the feature resolved experimentally at 11.0 meV lies in a region of high density of bulk states, where we do not find a distinct surface-localized mode, while Schmidt and Srivastava identified a state at 11.1 meV. Figure 2 of Ref. 31 indicates that a coupling of this mode to bulk vibrations probably changes its frequency only to a small extent.

Our $\overline{\Gamma}$ point phonon at 9.5 meV corresponds to a nearly dispersionless mode that can be resolved in both directions. This vibrational state is particularly interesting since it is related to a branch detected for the clean surface by means of HAS.[37,38] In contrast with our results for the pristine

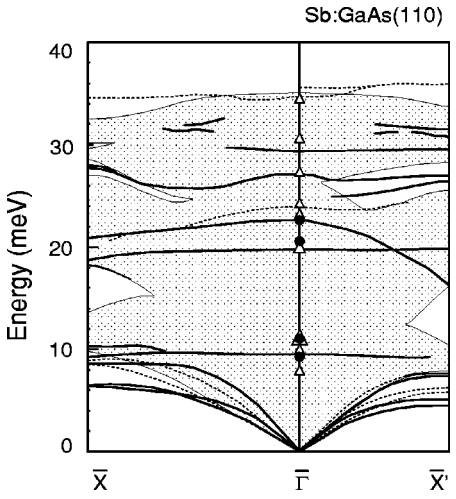

FIG. 3. Phonon dispersion computed for the ECL structure of Sb:GaAs(110). Surface-localized modes are indicated by solid lines; dotted lines represent vibrational modes of the clean surface. Triangles: frequencies determined in the frozen-phonon calculation of Ref. 21. Filled circles: experimental data from Raman scattering (Refs. 24 and 25).

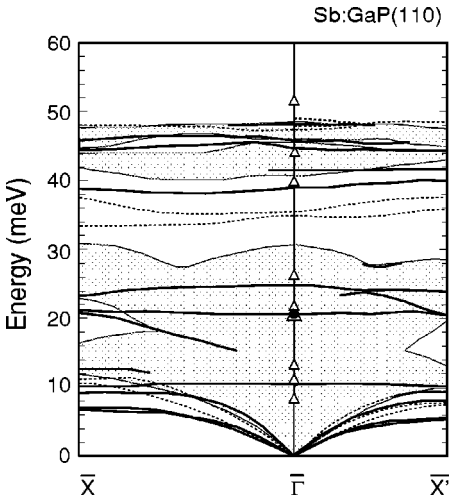

FIG. 4. Phonon dispersion computed for the ECL structure of Sb:GaP(110). Surface-localized modes are indicated by solid lines; dotted lines represent vibrational modes of the clean surface. Triangles: frequencies determined in the frozen-phonon calculation of Ref. 21. Filled circles: experimental data from Raman scattering (Ref. 24).

surface,[42] it can be clearly identified as a surface-localized state for the Sb:GaAs(110) surface. As discussed in Sec. IV B, a similar mode is present in the spectrum of Sb:GaP(110). In the region below the flat branch, there are three acoustic phonon modes. Our computations yield two nearly degenerate vibrations in the dispersion along the adatom zigzag chains with $\overline{X}$ point frequencies of 6.3 and 6.4 meV. The third branch has a zone-boundary energy of 8.84 meV. In the $\overline{\Gamma X'}$ direction, two branches of phonons with sagittal polarization are present. We obtain 4.6 and 7.4 meV for the frequencies at the zone boundary. The third mode has shear-horizontal polarization and an energy of 5.0 meV at the $\overline{X'}$ point.

B. Phonon dispersion of Sb:GaP(110)

The phonon dispersion calculated for Sb:GaP(110) is illustrated in Fig. 4. Only one distinct phonon mode could be measured by Raman spectroscopy at 20.7 meV.[24] We obtain 20.9 meV for this A'' mode, in good agreement with the experimental result and the vibrational energy of 20.8 meV determined by Schmidt and Srivastava.[21] In analogy with Sb:GaAs(110), we find three acoustic surface phonon modes for Sb:GaP(110) in both directions. The zone-boundary frequencies are 6.8, 7.1, and 9.3 meV at the $\overline{X}$ point and 5.4, 5.6, and 8.2 meV at the $\overline{X'}$ point.

A remarkable vibrational feature is the flat mode with a zone-center energy of about 10.7 meV. The frozen-phonon approach of Schmidt and Srivastava predicted its vibrational energy to be 11.1 meV. For clean GaP(110) no phonon with strong surface localization could be detected in this region. The eigenvector of the mode at 10.7 meV is illustrated in Fig. 5. It is characterized by normal displacements of the atoms in the adsorption layer and several substrate layers below. The eigenvector of the corresponding mode of Sb:GaAs(110) determined at 9.5 meV has essentially the same vibrational pattern. The displacement pattern is closely related to the atomic shifts that characterize the relaxation of the III-V(110) surfaces.

Restricting the atomic motion to a smaller number of layers does not drastically change the vibrational energy, as can be seen by comparing the frequency determined in our approach and that of Ref. 21. This is consistent with the fact that the rotational mode's frequency for a large variety of III-V(110) surfaces could already be estimated with reasonable accuracy in the tight-binding approach of Wang and Duke,[36] although coupling to substrate vibrations was neglected in their predictions.

The rotational mode was discussed in a series of theoretical investigations with an appreciable degree of controversy.[36,39–43,45] The eigenvector of the phonon state determined for Sb:GaP(110) provides clarification. For clean (110) surfaces, the rotational oscillation lies in a region of

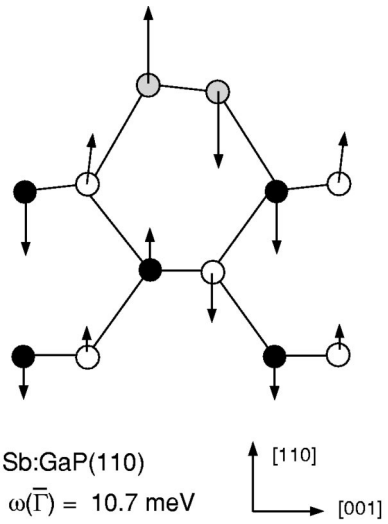

FIG. 5. Displacement pattern of the rotational mode in Sb:GaP(110) in a side view of the first four atomic layers.

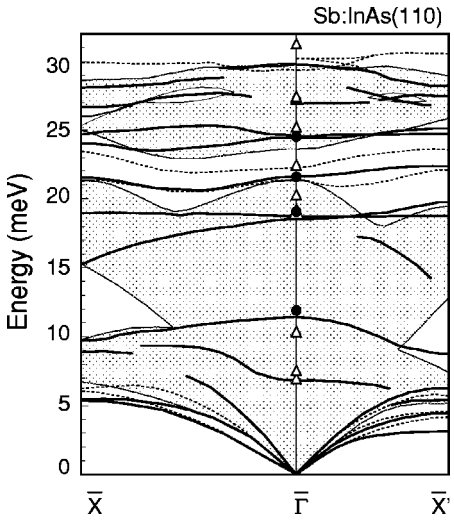

FIG. 6. Phonon dispersion computed for the ECL structure of Sb:InAs(110). Surface-localized modes are indicated by solid lines; dotted lines represent vibrational modes of the clean surface. Triangles: frequencies determined in the frozen-phonon calculation of Ref. 21. Filled circles: experimental data from Raman scattering (Ref. 27).

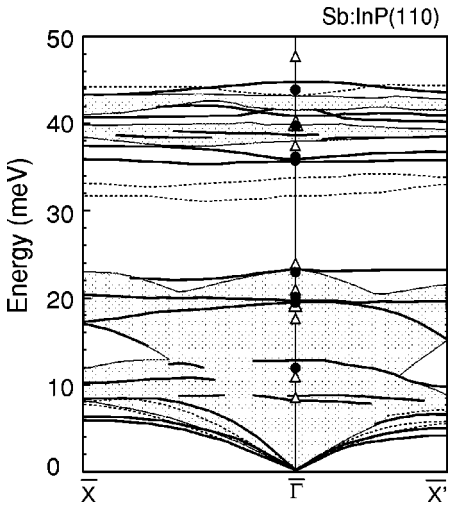

FIG. 7. Phonon dispersion computed for the ECL structure of Sb:InP(110). Surface-localized modes are indicated by solid lines; dotted lines represent vibrational modes of the clean surface. Triangles: frequencies determined in the frozen-phonon calculation of Ref. 21. Filled circles: experimental data from Raman scattering (Ref. 24).

high bulk density of states. It is therefore characterized by strong hybridization with bulk vibrations. As a result of the adsorption, the frequency of the rotational mode is substantially reduced because of the large mass of Sb. It is shifted below the region of high density of bulk states. In particular, for Sb:GaP(110), the mode couples only weakly with the vibrations of the substrate. Consequently, it is largely surface localized.

C. Phonon dispersion of Sb:InAs(110)

Figure 6 illustrates the phonon dispersion determined for Sb:InAs(110). By Raman spectroscopy, three A' modes were resolved at 11.9, 21.6, and 24.5 meV, and one vibration with A'' character at 19.1 meV.[27] These values compare very well with our surface vibrational energies of 11.4, 18.7, 21.7, and 24.5 meV. In addition, we obtain five more modes at 6.8, 18.6, 24.5, 26.9, and 29.9 meV. We find two acoustic phonon modes along the $\overline{\Gamma X}$ direction having the same zone-boundary energy of 5.4 meV. Our computations yield three acoustic branches for the $\overline{\Gamma X'}$ direction with end-point energies of 3.1, 4.5, and 6.3 meV.

In marked contrast with Sb:GaAs(110) and Sb:GaP(110), no clear indication is given for a flat branch that corresponds to a rotational mode. The vibration found in our computations at 6.8 meV exhibits atomic displacements along the adlayer zigzag chains. The rotational mode obtained in the frozen-phonon calculations at 7.5 meV mixes strongly with vibrations of the substrate and cannot be identified when allowing unrestricted dynamics. One can easily understand this behavior in terms of the mass relation between the atoms in the surface region. The frequency of the rotational mode is reduced only slightly by the adsorption of Sb on InAs(110), because of the small mass difference between In and Sb. We checked this by computing the vibrational modes for a Bi overlayer. This was done under the assumption that the structural details and the bond strengths of a Bi adlayer are exactly the same as those determined for Sb. Within this mass approximation, a localized phonon mode similar to that illustrated in Fig. 5 is predicted for Bi:InAs(110) with an energy of 6.8 meV.

D. Phonon dispersion of Sb:InP(110)

Detailed information from Raman spectroscopy[24] is available particularly for Sb:InP(110), as illustrated in Fig. 7. Two A'' modes were found at 20.0 and 36.0 meV, while six A' modes were detected at 11.9, 19.5, 22.9, 35.8, 39.8, and 43.9 meV. Our DFPT computations yield the energies 19.4 and 35.5 meV for the respective A'' modes and 12.6, 19.6, 23.0, 35.9, 40.8, and 44.7 meV for the corresponding states with A' character.

For the majority of the vibrational energies, there is also good agreement of our results with those of the frozen-phonon calculation of Schmidt and Srivastava. However, large deviations occur for the A'' mode detected by Raman scattering at 36.0 meV. The frequency determined by means of our DFPT calculations compares well with the experimental value but is in contrast with 40.3 meV obtained in the restricted dynamical model of Ref. 21.

The vibrational pattern labeled as A_2' in Fig. 8 illustrates a sagittally polarized mode determined in our computations for Sb:InP(110) at 35.9 meV. It mainly consists of atomic oscillations of P atoms in the second atomic layer. Vibrations in deeper layers are negligible. This mode is related to the lower gap mode of the clean InP(110) surface, as can be seen from Fig. 7 of Ref. 43. By means of their frozen-phonon approach, Schmidt and co-workers[41] obtained two vibrational states for the pristine InP(110) surface at 34.2 and 36.0 meV, while DFPT predicted two modes at 32.0 and 33.9 meV. The two vibrational states were recently resolved for InP(110) by Raman spectroscopy with zone-center energies of 31.5 and 33.6 meV.[56] Our results show that the eigenvector of the lower gap mode is only slightly influenced by the

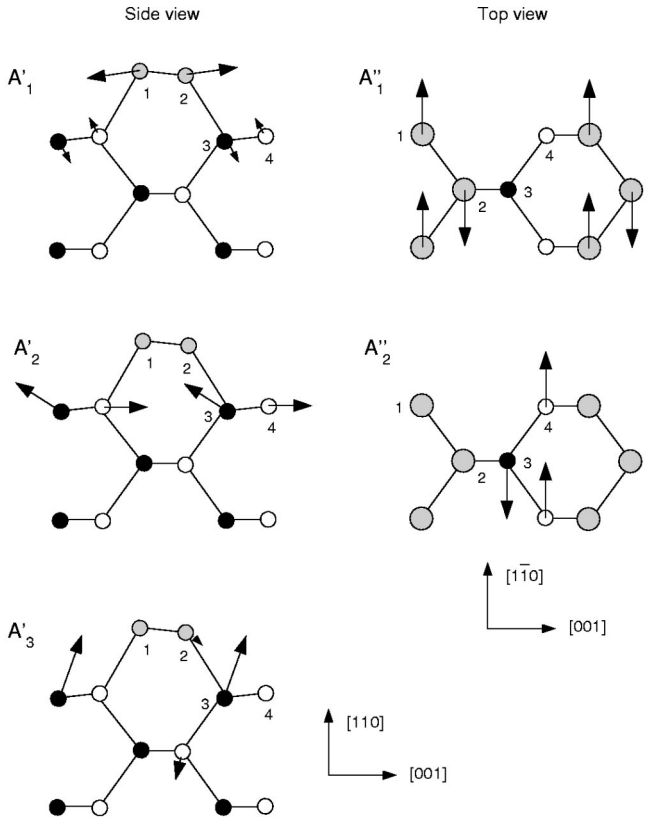

FIG. 8. Side and top views of optical zone-center phonon displacement patterns that are characteristic for all Sb:III-V(110) surfaces. Corresponding atoms in the side and top views are numbered. The frequencies computed for the modes of Sb adsorbed on GaAs, GaP, InAs, and InP are summarized in Table IV.

presence of the Sb overlayer. In Sb:InP(110) the oscillation of the first-substrate-layer P atoms includes Sb-P bonds, in addition. Therefore, the vibrational energy is increased from 32.0 meV to 35.9 meV. Under the assumption that the energy of the respective vibrational mode determined within the frozen-phonon approach should be increased by about 4 meV, one would expect a surface vibrational state at 38.2 meV. Actually, Schmidt and Srivastava find a corresponding state at 37.5 meV.

E. Comparison and trends

The Sb-covered (110) surfaces of GaAs, GaP, InAs, and InP have a series of overlayer modes, vibrations of the substrate and the interface which are characterized by very similar displacement patterns irrespective of the particular substrate. Figure 8 illustrates the five zone-center modes that are abundant in each of the considered adsorption systems. The only exception is the A_3' mode, which hybridizes strongly with bulk vibrations on the GaAs(110) surface. In Table IV, the phonon energies of the five characteristic states are summarized. In contrast with our results, Schmidt and Srivastava have compiled a total of six A' and three A'' modes.[21] Our modes labeled as A_1', A_3', A_1'', and A_2'' correspond to the modes $3A'$, $6A'$, $2A''$, and $3A''$ of Ref. 21. The frequencies of our A_2' feature are consistently in better agreement with the vibrational energies of the $5A'$ modes of Schmidt and Srivastava than with those of their $4A'$ oscillations.

TABLE IV. Vibrational energies (in meV) of the zone-center phonon modes illustrated in Fig. 8. Resonant modes are indicated by parentheses.

Mode	GaAs	GaP	InAs	InP
A_1'	(21.1)	22.8	21.7	23.0
A_2'	26.6	39.0	24.5	35.9
A_3'		48.5	29.9	44.7
A_1''	19.7	20.9	18.7	19.4
A_2''	29.3	41.6	24.6	35.5

There are always surface vibrational states found by DFPT that are close to the modes $2A'$ and $4A'$ of Ref. 21 as can be seen in Figs. 3, 4, 6, and 7. In some cases, these modes are rather resonant phonon states. This does not allow us to identify a distinct character for these vibrations. For such modes, it is not possible to follow their dispersion in all directions of the Brillouin zone.

We find the rotational mode ($1A'$ in Ref. 21) illustrated in Fig. 5 to be a strongly localized state in Sb:GaP(110). It can be identified as a clear surface state also for Sb:GaAs(110). However, a rotational motion with a similar degree of surface localization is not found for Sb:InP(110) and Sb:InAs(110). The high density of bulk states leads to a strong hybridization of the rotational mode with substrate vibrations. The mixing changes its frequency only to a minor extent. However, the displacement pattern is drastically influenced. Therefore, this mode is visible in restricted dynamical models but not in computations that take into account all degrees of freedom. It is also important to note that the energy of the rotational mode does not change with the relaxation angle. This was clearly seen for hydrogen-covered III-V(110) surfaces.[44,47] The frequency of the rotational mode can be effectively tuned by changing the atomic masses. It is strongly localized in cases where the (110) surfaces are covered by heavy atoms adsorbed in the ECL structure. This is concluded form our results obtained for Sb adsorbed on the III-V(110) surfaces and for the adsorption of Bi on InAs(110).

The frequencies of the A_2', A_1'', and A_2'' modes summarized in Table IV show clear trends: For a given adsorption system, the frequency of the A_2' mode is almost the same as that of the A_2'' mode. Both states are characterized by an out-of-phase vibration of the first-substrate layer atoms. In the A_2' mode, the atomic motions are polarized in the $(1\bar{1}0)$ plane, while the atoms vibrate parallel to the Sb-overlayer chains in the A_2'' mode. The shear vibration A_1'' is strongly localized in the adsorption layer. Its frequency is essentially determined by the strength of the bonds between the overlayer atoms and their masses. The frequency of this mode is the largest for Sb:GaP(110) and the smallest for Sb:InAs(110), in complete consistency with Fig. 2, which illustrates the Sb-Sb bond lengths as a function of the substrate lattice constant. In principle, one might expect a similar trend for the A_1' vibrations. However, the frequencies behave in a slightly different way, since this mode also includes oscillations of the atoms in the first substrate layer.

An interesting question in the comparison of the clean and adsorbate covered surfaces is focused on the behavior of the

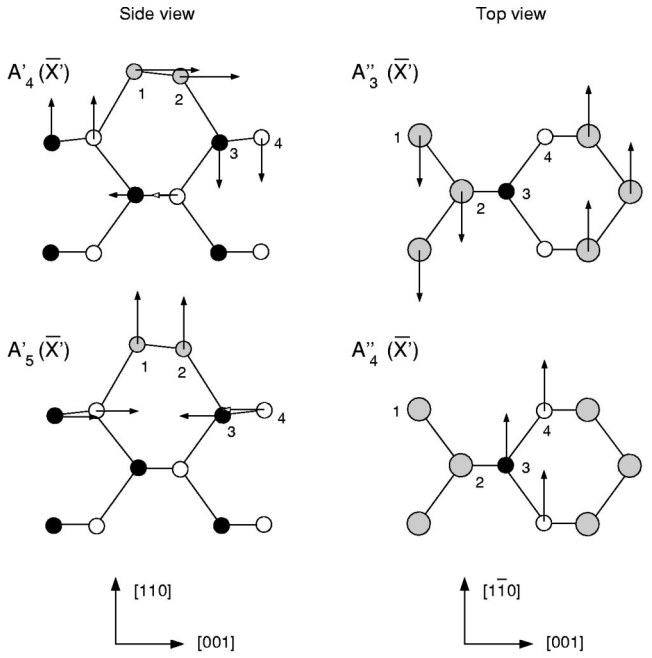

FIG. 9. Side and top views of displacement patterns of acoustic zone-boundary phonon modes determined for the Sb:III-V(110) surfaces. Corresponding atoms in the side and top views are numbered. The frequencies computed for the modes of Sb adsorbed on GaAs, GaP, InAs, and InP are summarized in Table V.

gap modes. The adsorption of Sb changes the phonon dispersion in the gap between the acoustic and optical vibrations of the bulk in particular for GaP and InP(110), as indicated by the dotted lines shown in Figs. 4, 6, and 7. As already discussed in Sec. IV D, the frequency of the lower gap mode is increased by about 5 meV through the adsorption. The corresponding vibrational state of the adsorption system is the A_2' mode. The upper gap mode of the pristine surfaces is shifted into the continuum of optical bulk vibrations so that the corresponding state cannot be identified. For clean and hydrogen-covered surfaces it was predicted that the energy of the lower gap mode decreases as a result of the derelaxation.[43,44,47] The additional bonds between the first substrate-layer atoms and the heavy Sb-overlayer atoms, however, finally lead to an increase of the vibrational energy.

It is interesting to note that our A_1' mode computed for Sb:InAs(110) has nearly the same energy and dispersion as the lower gap mode of the clean surface along the $\overline{\Gamma X}$ direction. Also the eigenvectors are essentially the same, assuming that the two Sb atoms simply substitute for In and As. The oscillation involves all atoms of the outermost two layers. The larger mass of Sb should lead to a slight reduction of the vibrational energy. It may be concluded from the frequency of the A_1' mode that the bonds between the adsorption layer and the substrate are strong enough to compensate the mass effect.

The frozen-phonon calculations of Schmidt and Srivastava yield a low-frequency shear mode labeled as $1A''$ in Ref. 21. In this mode, the zigzag chains of the substrate and the overlayer move as separate rigid units in the direction of their orientation. The vibration mainly consists of an oscillation of the first-substrate layer chains against the zigzag chains in the adlayer and the second substrate layer. From our DFPT calculations, we obtain two shear horizontally polarized low-energy phonon modes at the $\overline{X'}$ point. Their diplacement patterns are illustrated in Fig. 9. For Sb:InAs(110) and Sb:InP(110), the $A_4''(\overline{X'})$ feature can indeed be related to $1A''$-like shear modes at the $\overline{\Gamma}$ point with energies of 6.8 and 8.1 meV, respectively.

TABLE V. Vibrational energies (in meV) of the zone-boundary phonon modes illustrated in Fig. 9. Resonant modes are indicated by parentheses.

Mode	GaAs	GaP	InAs	InP
$A_4'(\overline{X'})$	4.6	5.4	3.1	4.0
$A_5'(\overline{X'})$	7.4	8.2	(6.3)	
$A_3''(\overline{X'})$	5.0	5.6	4.5	4.9
$A_4''(\overline{X'})$	7.5	9.5	5.4	6.4

Table V summarizes the frequencies obtained from our computations for the four lowest surface phonon modes at the $\overline{X'}$ point. The frequencies of the corresponding three phonon modes of the clean surfaces are significantly higher, as illustrated by the dotted lines in Figs. 3, 4, 6 and 7. The difference results from the large atomic mass of Sb and the surface localization of the acoustic phonon modes close to the zone-boundary points. There are two modes with shear horizontal polarization in the dispersion along the $\overline{\Gamma X'}$ direction, while only one respective phonon branch appears in the dispersion of the pristine surfaces.[42–44] The shear mode $A_3''(X')$ resembles that of the uncovered surfaces. The vibrational state $A_4''(\overline{X'})$ can also be derived from the shear-horizontal mode of the clean surfaces. The adsorption of the heavy Sb atoms enhances the restoring forces for substrate-layer displacements and hence increases the respective vibrational energy. For smaller wave vectors, the $A_4''(\overline{X'})$ mode becomes resonant. It can be related to $\overline{\Gamma}$-point vibrations only for Sb adsorbed on InAs and InP(110).

V. SUMMARY

In this paper, we have presented the results from *ab initio* linear-response calculations for the phonon dispersion of the ECL structure of Sb adsorbed on the (110) surfaces of GaAs, GaP, InAs, and InP. Our dispersion curves are in good agreement with all existing experimental data available for these systems.

Our computations yield five localized phonon modes at the $\overline{\Gamma}$ point characterizing the ECL structure of the Sb adsorption. The displacement patterns of these modes are essentially independent on the particular substrate. The calculated vibrational energies compare very well with the results obtained by means of the frozen-phonon method[21] and the experiments.[10,12,13,24,26,27] The additional modes found in the previous computations are not localized for all of the Sb:III-V(110) surfaces considered in our study.

Our results provide important new insights into the nature of the rotational mode. This vibrational feature was proposed by early tight-binding total-energy calculations,[36] in order to provide an interpretation for the flat branch detected by HAS

in the dispersion of the clean GaAs(110) surface about one decade ago.[37,38] Successive computations indicated that the frequency of the rotational oscillation is essentially independent of the relaxation angle. Our present study shows that the energy of this vibration can be effectively tuned by changing the atomic masses in the surface region. This allows one to make the rotational mode clearly visible by covering the (110) surfaces of GaAs and GaP with Sb. For Sb:InP(110) and Sb:InAs(110), however, the mode is still largely resonant.

The probably most characteristic vibrational feature of the one-monolayer ECL structure is the nearly dispersionless shear mode A_1''. Its frequency scales with the inverse of the Sb-Sb bond length, which is primarily predetermined by the substrate lattice constant. This is completely consistent with the frequencies measured by Raman spectroscopy for the shear modes.

Finally, the energy of the two gap modes characterizing the clean surfaces of GaP, InP, and InAs is drastically changed as a result of Sb adsorption. The upper gap mode is shifted upwards into the continuum of the optical bulk vibrations. The energy of the lower gap mode is increased by about 5 meV.

ACKNOWLEDGMENTS

This work was supported by the Deutsche Forschungsgemeinschaft through a Habilitationsstipendium (FR 1426/2-1). We are indebted to S. Baroni, P. Giannozzi, and A. Testa for providing numerical support.

[1] P. Skeath, C.Y. Su, I. Lindau, and W.E. Spicer, J. Vac. Sci. Technol. **17**, 874 (1980).
[2] J. Carelli and A. Kahn, Surf. Sci. **116**, 380 (1982).
[3] C.B. Duke, A. Paton, W.K. Ford, A. Kahn, and J. Carelli, Phys. Rev. B **26**, 803 (1982).
[4] W.K. Ford, T. Guo, S.L. Lantz, K. Wang, S.L. Chang, C.B. Duke, and D.L. Lessor, J. Vac. Sci. Technol. B **8**, 940 (1990).
[5] N. Esser, D.R.T. Zahn, C. Müller, W. Richter, C. Stephens, R. Whittle, I.T. McGovern, S. Kulkarni, and W. Braun, Appl. Surf. Sci. **56-59**, 169 (1992).
[6] C. Nowak, A. Chassé, A. Hempelmann, W. Richter, E. Dudzik, R. Whittle, I.T. McGovern, W. Braun, and D.R.T. Zahn, Surf. Sci. **307-309**, 685 (1994).
[7] C. Nowak, A. Hempelmann, A. Märkl, A. Chassé, E. Dudzik, C. Müller, I.T. McGovern, W. Braun, W. Richter, and D.R.T. Zahn, Surf. Sci. **331-333**, 564 (1995).
[8] C. Nowak, J. Krujatz, A. Märkl, C. Meyne, A. Chassé, W. Braun, W. Richter, and D.R.T. Zahn, Surf. Sci. **331-333**, 619 (1995).
[9] J.C. Patrin, Y.Z. Li, M. Chander, and J.H. Weaver, Phys. Rev. B **46**, 10 221 (1992).
[10] W.K. Ford, T. Guo, D.L. Lessor, and C.B. Duke, Phys. Rev. B **42**, 8952 (1990).
[11] W.K. Ford, T. Guo, K.-J. Wan, and C.B. Duke, Phys. Rev. B **42**, 11 896 (1990).
[12] C. Nowak, Ph.D. thesis, Berlin University of Technology, 1996.
[13] C. Nowak, A. Chassé, W. Braun, W. Richter, I.T. McGovern, and D.R.T. Zahn, J. Electron Spectrosc. Relat. Phenom. **80**, 143 (1996).
[14] W.K. Ford, T. Guo, K.-J. Wan, and C.B. Duke, Phys. Rev. B **45**, 11 896 (1995).
[15] K.E. Miyano, J.C. Woicik, T. Kendelewicz, W.E. Spicer, M. Richter, and P. Pianetta, Phys. Rev. B **47**, 6444 (1993).
[16] M.G. Betti, C. Mariani, N. Jedrecy, R. Pinchaux, A. Ruocco, and M. Sauvage-Simkin, Phys. Rev. B **50**, 14 336 (1994).
[17] J.P. LaFemina, Surf. Sci. Rep. **16**, 133 (1992).
[18] G.P. Srivastava, J. Phys.: Condens. Matter **5**, 4695 (1993).
[19] G.P. Srivastava, Phys. Rev. B **47**, 16 616 (1993); Surf. Sci. **307-309**, 328 (1994).
[20] W.G. Schmidt, B. Wenzien, and F. Bechstedt, Phys. Rev. B **49**, 4731 (1994); Surf. Sci. **307-309**, 235 (1994).
[21] W.G. Schmidt and G.P. Srivastava, Surf. Sci. **331-333**, 540 (1995).
[22] W.G. Schmidt, F. Bechstedt, and G.P. Srivastava, Surf. Sci. Rep. **25**, 141 (1996).
[23] N. Esser, M. Reckzügel, R. Srama, U. Resch, D.R.T. Zahn, W. Richter, C. Stephens, and M. Hünermann, J. Vac. Sci. Technol. B **8**, 680 (1990).
[24] M. Hünermann, Ph.D. thesis, Aachen University of Technology, Germany, 1990; M. Hünermann, L. Geurts, and W. Richter, Phys. Rev. Lett. **66**, 640 (1991).
[25] W. Richter, N. Esser, A. Kelnberger, and M. Köpp, Solid State Commun. **84**, 165 (1992).
[26] N. Esser, M. Köpp, P. Haier, and W. Richter, J. Electron Spectrosc. Relat. Phenom. **64/65**, 85 (1993).
[27] N. Esser, M. Köpp, P. Haier, and W. Richter, Phys. Status Solidi A **152**, 191 (1995).
[28] T.J. Godin, J.P. LaFemina, and C.B. Duke, J. Vac. Sci. Technol. B **4**, 2282 (1991).
[29] G.K. Schenter and J.P. LaFemina, J. Vac. Sci. Technol. A **10**, 2429 (1991).
[30] W.G. Schmidt and G.P. Srivastava, Solid State Commun. **89**, 345 (1994).
[31] P.V. Santos, N. Esser, M. Cardona, W.G. Schmidt, and F. Bechstedt, Phys. Rev. B **52**, 12 158 (1995).
[32] N. Esser, K. Hinrichs, and W. Richter (private communication).
[33] W. Theis, H. Tröger, G. König, and K. H. Rieder (private communication).
[34] S. Baroni, P. Giannozzi, and A. Testa, Phys. Rev. Lett. **58**, 1861 (1987).
[35] P. Giannozzi, S. de Gironcoli, P. Pavone, and S. Baroni, Phys. Rev. B **43**, 7231 (1991).
[36] Y.R. Wang and C.B. Duke, Surf. Sci. **205**, L755 (1988).
[37] U. Harten and J.P. Toennies, Europhys. Lett. **4**, 833 (1987).
[38] R.B. Doak and N.B. Nguyen, J. Electron Spectrosc. Relat. Phenom. **44**, 205 (1987).
[39] P. Santini, L. Miglio, G. Benedek, and P. Ruggerone, Surf. Sci. **241**, 346 (1991).
[40] R. Di Felice, A.I. Shkrebtii, F. Finocchi, C.M. Bertoni, and G. Onida, J. Electron Spectrosc. Relat. Phenom. **64/65**, 697 (1993).
[41] W.G. Schmidt, F. Bechstedt, and G.P. Srivastava, Phys. Rev. B **52**, 2001 (1995).
[42] J. Fritsch, P. Pavone, and U. Schröder, Phys. Rev. Lett. **71**, 4194 (1993).

[43] J. Fritsch, P. Pavone, and U. Schröder, Phys. Rev. B **52**, 11 326 (1995).
[44] C. Eckl, J. Fritsch, P. Pavone, and U. Schröder, Surf. Sci. **394**, 47 (1997).
[45] J. Fritsch, C. Eckl, P. Pavone, and U. Schröder, in: *Festkörperprobleme, Advances in Solid State Physics*, edited by R. Helbig (Vieweg, Braunschweig, 1997), Vol. 36, p. 135.
[46] J. Fritsch and U. Schröder, Phys. Rep. **309**, 211 (1999).
[47] J. Fritsch, A. Eckert, P. Pavone, and U. Schröder, J. Phys.: Condens. Matter **7**, 7717 (1995).
[48] P. Hohenberg and W. Kohn, Phys. Rev. **136**, B864 (1964).
[49] W. Kohn and L.J. Sham, Phys. Rev. A **140**, A1133 (1965).
[50] D.M. Ceperley and B.I. Alder, Phys. Rev. Lett. **45**, 566 (1980).
[51] J. Perdew and A. Zunger, Phys. Rev. B **23**, 5048 (1981).
[52] G.B. Bachelet, D.R. Hamann, and M. Schlüter, Phys. Rev. B **26**, 4199 (1982).
[53] N. Troullier and J.L. Martins, Phys. Rev. B **43**, 1993 (1991).
[54] L. Pavesi, P. Giannozzi, and F.K. Reinhart, Phys. Rev. B **42**, 1864 (1990); W. Andreoni, G. Pastore, R. Car, M. Parrinello, and P. Giannozzi, *Band Structure Engineering in Semiconductor Microstructures*, Vol. 189 of NATO Advanced Study Institute, Series B: Physics, edited by R.A. Abram and M. Jaros (Plenum, New York, 1998), p. 129.
[55] J.L.A. Alves, J. Hebenstreit, and M. Scheffler, Phys. Rev. B **44**, 6188 (1991).
[56] K. Hinrichs, A. Schierhorn, P. Haier, N. Esser, W. Richter, and J. Sahm, Phys. Rev. Lett. **79**, 1094 (1997).